

1 Evidence for the Chemical Mechanism of RibB (3,4-Dihydroxy-2- 2 butanone 4-phosphate Synthase) of Riboflavin Biosynthesis

3 Nikola Kenjić, Kathleen M. Meneely, Daniel J. Wherritt, Melissa C. Denler, Timothy A. Jackson,
4 Graham R. Moran, and Audrey L. Lamb*



Cite This: <https://doi.org/10.1021/jacs.2c03376>



Read Online

ACCESS |



Metrics & More

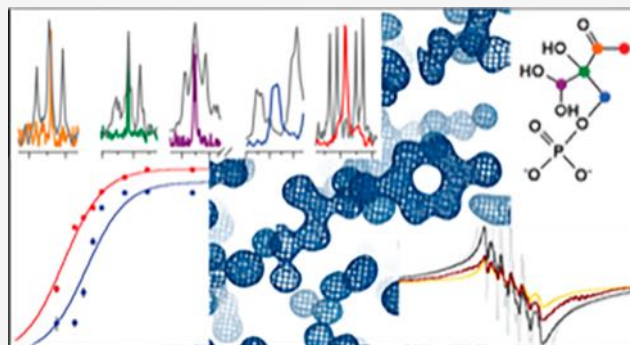


Article Recommendations



Supporting Information

5 **ABSTRACT:** RibB (3,4-dihydroxy-2-butanone 4-phosphate syn-
6 thase) is a magnesium-dependent enzyme that excises the C4 of D-
7 ribulose-5-phosphate (D-Ru5P) as formate. RibB generates the
8 four-carbon substrate for lumazine synthase that is incorporated
9 into the xylene moiety of lumazine and ultimately the riboflavin
10 isoalloxazine. The reaction was first identified by Bacher and co-
11 workers in the 1990s, and their chemical mechanism hypothesis
12 became canonical despite minimal direct evidence. X-ray crystal
13 structures of RibB typically show two metal ions when solved in the
14 presence of non-native metals and/or liganding non-substrate
15 analogues, and the consensus hypothetical mechanism has
16 incorporated this cofactor set. We have used a variety of
17 biochemical approaches to further characterize the chemistry
18 catalyzed by RibB from *Vibrio cholera* (VcRibB). We show that full activity is achieved at metal ion concentrations equal to the
19 enzyme concentration. This was confirmed by electron paramagnetic resonance of the enzyme reconstituted with manganese and
20 crystal structures liganded with Mn^{2+} and a variety of sugar phosphates. Two transient species prior to the formation of products
21 were identified using acid quench of single turnover reactions in combination with NMR for singly and fully ^{13}C -labeled D-Ru5P.
22 These data indicate that dehydration of C1 forms the first transient species, which undergoes rearrangement by a 1,2 migration,
23 fusing C5 to C3 and generating a hydrated C4 that is poised for elimination as formate. Structures determined from time-dependent
24 Mn^{2+} soaks of VcRibB-D-Ru5P crystals show accumulation in crystallo of the same intermediates. Collectively, these data reveal for
25 the first time crucial transient chemical states in the mechanism of RibB.



26 ■ INTRODUCTION

27 Riboflavin is the direct precursor for the production of flavin
28 adenine mononucleotide and subsequently flavin adenine
29 dinucleotide, essential cofactors in redox and non-redox
30 reactions in all forms of life.^{1,2} Riboflavin is required for
31 fundamental cellular processes, such as primary metabolism,
32 the electron transport chain of cellular respiration, folate
33 synthesis,¹ iron absorption,³ DNA repair,⁴ and inflammation/
34 immune responses.^{5,6} Plants and bacteria have genes for the
35 enzymatic production of riboflavin, but animals must obtain
36 riboflavin (vitamin B2) from their diet. Not surprisingly,
37 riboflavin biosynthesis has drawn attention as a target for
38 antibacterial/antimicrobial drug design.^{7–9}

39 Riboflavin biosynthesis has a convergent pathway with the
40 initial substrates of the individual branches being guanosine
41 triphosphate and D-ribulose 5-phosphate (D-Ru5P, a five-
42 carbon sugar phosphate of the pentose phosphate pathway),
43 both prevalent metabolites. 3,4-Dihydroxy-2-butanone 4-
44 phosphate (DHBP) synthase, or RibB, is a magnesium-
45 dependent enzyme that dehydrates the first carbon and
46 removes the fourth carbon of D-Ru5P to make the four-

carbon, DHBP product (Figure 1A). Evidence for this 47 fl
unexpected chemistry is from classic biochemistry feeding 48
studies and endpoint assays with ^{13}C -labeled ribose, acetate, 49
glucose, glycerol, and ribulose-5-phosphate employing ^{13}C 50
NMR detection.^{10–16} The enzyme mechanism that has been 51
proposed is necessarily complicated and requires at least four 52
steps: (1) dehydration at C1 to generate the methyl, (2) a 53
skeletal rearrangement to link C3 and C5, and a (3) hydration 54
at C4 to facilitate (4) deformylation. The order of events as 55
accepted in the literature is shown in Figure 1B,¹⁶ which we 56
refer to as the “canonical” mechanism. The inversion of the 57
stereochemistry at C3 has previously been established by CD 58
spectroscopy (Figure 1A).¹⁵ Due to the complexity of the 59
reaction, it is not surprising that the RibB reaction is 60

Received: March 29, 2022

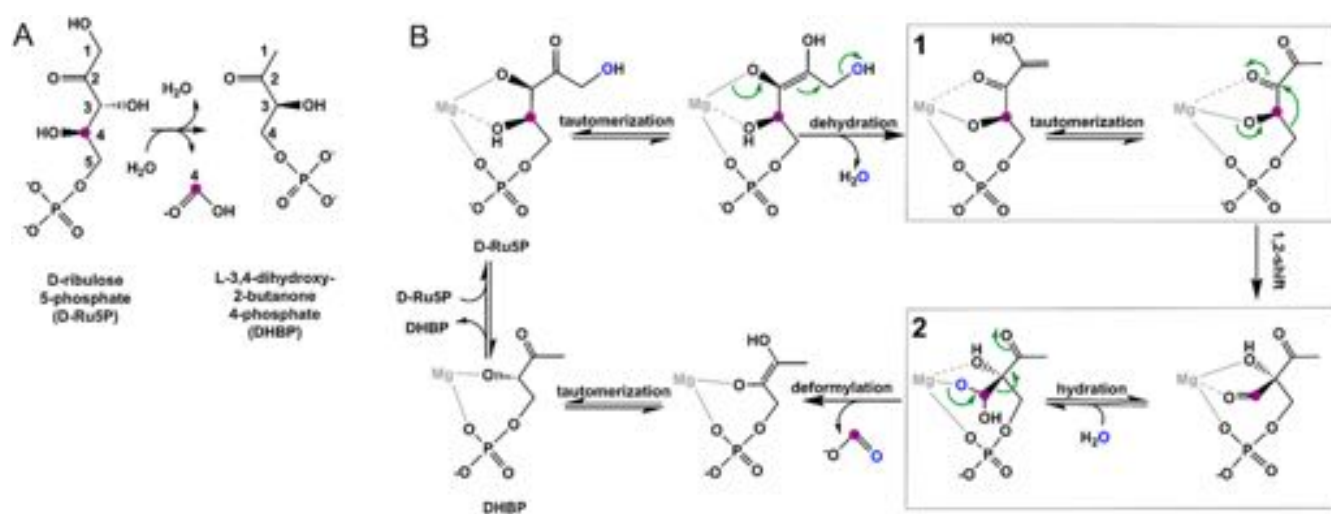


Figure 1. Hypothetical canonical mechanism depicted in the context of the findings of this study. (A) RibB catalyzes the conversion of D-ribulose 5-phosphate (D-Ru5P) to L-3,4-dihydroxy-2-butanone 4-phosphate (DHBP), dehydrating C1 and removing C4 as formate. (B) Mechanism proposed in the literature has four key steps: dehydration, 1,2-shift, hydration, and deformylation. Boxes indicate intermediate states identified in this study. Structures drawn in the Natta projection.

61 considered to be one of the rate-limiting steps in riboflavin
62 biosynthesis,¹⁷ with RibB enzymes demonstrating turnover
63 numbers on the order of six per minute.¹⁸

64 The structure of RibB appears to be a standard $\alpha+\beta$
65 structure, in which α -helices pack against both sides of a
66 central β -sheet (Figure 2). However, the connectivity of the

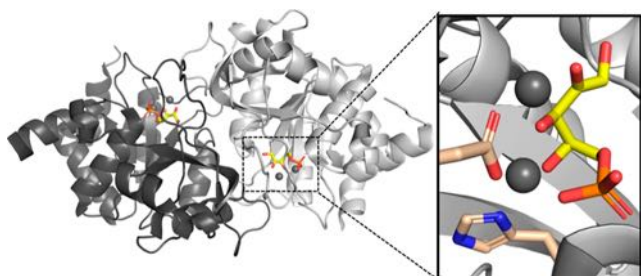


Figure 2. *V. cholerae* RibB structure (PDB: 4P8E). RibB is a dimer (monomers light and dark gray). This structure contains the D-Ru5P substrate (yellow sticks with red oxygens and orange phosphorous) and is inactive because the required magnesium ion(s) have been substituted by the two zinc ions (gray spheres). The inset shows magnification of the active site, highlighting two residues, Glu39 and His154 colored wheat, which coordinate to the two reported metal ions and will be shown in all subsequent images of the active site.

67 secondary structure is unique and dictates that RibB has a
68 distinctive fold.^{19–21} Indeed, if one performs a homology
69 search using PDBFold²² and sets low thresholds, 51 RibB
70 chains are returned with very high secondary structure
71 matching (over 80%) and strikingly similar root mean squared
72 deviation (rmsd) (1.5 Å or less for at least 180 of 216 C α
73 carbons). Additionally, four protein structures of unknown
74 function are identified, which show a clear deviation in
75 comparison statistics (rmsd doubles, Q score halves). The
76 active site is surrounded by two mobile loops. The shorter
77 loop, loop 1, is composed of acidic residues that are important
78 for binding of the substrate and metal. The longer loop, loop 2,
79 shows conformational flexibility with the substrate and metal
80 binding.^{20,21,23}

The majority of structures reported in the PDB are for non- 81
active states, with Mn²⁺, Zn²⁺, and Ca²⁺ substituted for the 82
catalytic Mg²⁺. Others have sulfate or phosphate in the active 83
site, and a few have a metal and/or substrate or substrate 84
analogues bound.^{19–21,23–28} It is widely accepted that the 85
enzyme requires two magnesium ions to be catalytically active, 86
but this is based on noncatalytic zinc-substituted structures of a 87
ternary protein–metal–substrate complex.^{23,27} However, 88
RibB-ribulose 5-phosphate complex structures show that the 89
substrate binds in the absence of metal with the phosphate 90
highly coordinated by amino acid side chains.²⁸ Indeed, there 91
are several structures in which sulfate or phosphate bind in the 92
substrate-phosphate site in the absence of metal, indicating 93
that the metal ion is not required for substrate binding.^{20,27} 94

We have sought to provide evidence for the chemical 95
mechanism of RibB. Initially, we determined that RibB uses a 96
mononuclear magnesium center for catalysis using perturba- 97
tion of tyrosine fluorescence, activity assays, and electron 98
paramagnetic resonance (EPR) data. Furthermore, we showed 99
that RibB activity is pH dependent, which correlates with 100
magnesium binding. Using acid quench of a single turnover 101
reaction in combination with nuclear magnetic resonance and 102
X-ray crystallography employing time-dependent crystal 103
soaked with the native substrate, we identified two catalytic 104
intermediates that accumulate in the catalytic cycle of RibB 105
that give credence to the hypothesis of a 1,2-shift followed by 106
deformylation for the excision of the 4-carbon from the 5- 107
carbon D-ribulose 5-phosphate. 108

109 METHODS

RibB Overexpression and Purification. The overexpression 110
construct for the RibB gene was prepared by GenScript. The ribB 111
gene from *Vibrio cholerae* (*V. cholerae*) (sequence ID: AE003853.1, 112
strain: N16961, taxid: 243277) was initially synthesized and cloned 113
into the pUC15 vector. This gene was then transferred to the pET28a 114
+ vector that yields the VcRibB protein with an N-terminal 6 His tag. 115
The VcRibB construct was transformed into BL21(DE3) *Escherichia* 116
coli (*E. coli*) (New England Biolabs) and grown overnight at 37 °C in 117
50 mL of LB broth, Miller (Fisher) with 50 μ g/mL kanamycin in a 118
shaker incubator (250 rpm). 1L of the Miller formulation of LB broth 119
with 50 μ g/mL kanamycin was inoculated with 10 mL of the 120

overnight culture and grown at 37 °C in a baffled flask in a shaker incubator (250 rpm). When the culture OD_{600nm} reached 0.8, protein expression was induced with a final concentration of 0.5 mM isopropyl β-D-1-thiogalactopyranoside (IPTG) and was further incubated at 37 °C for 4 h with shaking. The cells were harvested by centrifugation (6000g, 10 min, 4 °C). The cell pellet was resuspended in 10 mL of 50 mM Tris-HCl (pH 8.0), 50 mM imidazole, and 500 mM NaCl per liter of culture broth. Resuspended cells were lysed by passage through a French Press three times at 13,000 psi. The cell lysate was centrifuged at 12,000g for 40 min at 4 °C. The supernatant was injected onto a 25 mL Chelating Sepharose Fast Flow (GE Healthcare) column charged with nickel chloride and pre-equilibrated with 50 mM Tris-HCl (pH 8.0), 50 mM imidazole, and 500 mM NaCl. The protein was eluted with a 250 mL linear gradient increasing the imidazole concentration to 500 mM imidazole (RibB eluted at ~200 mM imidazole) or with a step gradient of 300 mM imidazole. The protein was concentrated to 30 mL using an Amicon nitrogen gas-pressurized concentrator with a 10 kDa cutoff filter and injected onto a 120 mL Superdex 200 gel-filtration column (GE Healthcare), pre-equilibrated with 25 mM Tris-HCl (pH 8.0). RibB eluted as a dimer and was concentrated using an Amicon Ultracell 30 K centrifugal concentrator to 40 mg/mL, as determined by Bradford, and stored at -80 °C for later use. The purification yield was 250 mg of protein per liter of culture.

RibB Purification in the Presence of EDTA. To remove the residual divalent metal ions, prior to the size exclusion step, the protein was incubated with a final concentration of 2 mM EDTA for 10 min on ice. The buffer for the size exclusion column contained 100 μM EDTA. Before binding and activity assay experiments commenced, the protein was exchanged again into freshly made 25 mM Tris-HCl (pH 8.0), 100 μM EDTA, and concentrated to 37.7 mg/mL using an Amicon Ultracell 30 K centrifugal concentrator.

Steady-State Kinetics Varying the D-Ribulose 5-Phosphate Concentration. We adapted the previously developed assay^{18,23} to compare the kinetic parameters of our purified enzyme for differing metals and sugar phosphates. A major change to assay included using the actual sugar phosphates as substrates as opposed to the addition of pentose phosphate isomerase to generate D-ribulose 5-phosphate during assay incubation. D-ribulose 5-phosphate (D-Ru5P), D-ribose 5-phosphate (D-R5P), D-xylulose 5-phosphate (D-Xy5P), and L-xylulose 5-phosphate (L-Xy5P) (Sigma-Aldrich) were dissolved in 50 mM Tris-HCl (pH 7.5) to a concentration of 90 mM. Sugar phosphate, 10 μM enzyme, and 10 mM MgCl₂ were mixed to a final volume of 200 μL and incubated for 30 min at room temperature with sugar phosphate concentrations varied from 0 to 4 mM for D-Ru5P, 0–200 mM for D-R5P, 0–8 mM for D-Xy5P, and 0–20 mM for L-Xy5P. The reaction was quenched by the addition of 175 μL of freshly made 200 mM naphthol (dissolved in 1 N NaOH) and 250 μL of 270 mM creatine (dissolved in water), and the color was allowed to develop for 30 min.¹⁸ The product was detected by an absorption scan from 450 nm to 650 nm using a Cary 50 Bio UV–visible spectrophotometer. The absorbance at λ_{max} (525 nm) was corrected by subtracting the absorbance at 650 nm and then converted to the concentration (in nM) using a 3,4-butadione standard curve, not the 3,4-dihydroxy-2-butanone phosphate (DHBP), as was carried out previously.¹⁸ Values for V_{max} and K_M are averages of three trials collected twice on separate days, and errors are reported as the standard deviation of these values. The data for the biological substrate (D-Ru-5P) and metals (Mg²⁺ and Mn²⁺) were fit to the Michaelis–Menten equation using Kaleidgraph (Synergy Software). The data for the other sugar phosphates were fit to the substrate inhibition model to give a trend line illustrative of the data, but numbers are not reported due to poor fit (see the Results section). Error propagation was used in the determination of error values for k_{cat} and k_{cat}/K_M. For the pH titration, D-Ru5P was the varied substrate, and a 100 mM succinic acid, phosphate, glycine (SPG) buffer system was used at pH values of 5.0, 5.4, 5.8, 6, 6.5, 7.0, 8.0, and 9.0, as described by Newman.²⁹ pH profiles of k_{cat} and k_{cat}/K_M values for substrates were fit to the following equation:

Kinetic parameters at each pH were determined in triplicate. The values presented are the averages of these three trials, and the reported errors are the standard deviation.

Steady-State Kinetics Varying the Metal Ion Concentration. The dependence of the steady-state kinetic parameters on the magnesium concentration was determined with D-Ru5P with one alteration in the procedure. The standard reaction mixture (200 μL) contained diluted MgCl₂ (Fisher 99.9% pure; 0–800 μM), 1.8 mM Ru5P, and 10 μM enzyme. The dependence of the steady-state kinetic parameters on the manganese concentration was obtained in the same manner as with Mg²⁺ but used 1 μM enzyme and pure MnCl₂ (Fisher 99% pure; 0–250 μM), and the incubation time prior to quenching was increased to 150 min.

Metal-Binding Stoichiometry. VcRibB has no tryptophan residues, and changes in intrinsic tyrosine fluorescence were used to observed metal binding. The data were measured using a Cary 50 Eclipse fluorometer with an excitation wavelength of 280 nm and emission recorded from 290 to 400 nm (excitation slit: 10 nm; emission slit: 5 nm). The 200 μL of the reaction mixture containing 50 mM tris-HCl (pH 7.5), 100 μM EDTA, 1.8 mM D-Ru5P, and 60 μM RibB [50 mM Tris-HCl, 100 μM EDTA (pH 8)] was titrated with 1 μL increments of 2 mM MgCl₂ and 100 μM EDTA solution. The reported Mg²⁺ concentration accounts for the dilution. Tyrosine fluorescence at 302 nm was corrected with the fluorescence for a control sample (titrated in the presence of 100 μM EDTA). Experiments were repeated three times, and data points reported are an average of three trials with the error reported as the standard deviation of the trials. For the pH-dependence of Mg binding, magnesium chloride was the varied component, and a 50 mM SPG buffer system was used for pH values of 4.5–9.0. Binding curves at each pH were determined in triplicate. The values presented are the averages of the three trials, and the reported errors are the standard deviation.

Circular Dichroism Spectroscopy. The spectra of each 200 μL sample containing 100 mM SPG buffer at pH 4–9 with 5 μM enzyme were collected using a Jasco J-1100 CD spectropolarimeter with a 1 mm pathlength. Each scan analyzed was an average of three scans at 50 nm/min with a 1.00 nm bandwidth and a digital integration time (D.I.T.) of 4 s. Data were collected from 185 to 260 nm at 0.1 nm intervals.

Metal Stoichiometry Evaluated from RibB Activity. In each reaction mixture of 200 μL, the final concentration of components was 50 mM Tris-HCl (pH 7.5), 100 μM EDTA, and 1.8 mM D-Ru5P. MgCl₂ was titrated in successive assays in increments of 20 μM from 0 to 220 μM. The reaction was initiated by the addition of 60 μM RibB protein purified in the presence of EDTA and incubated for 1 h at room temperature. Steady-state data were calculated using the above procedure. The experiment was repeated three times, and values reported are the averages of three trials with errors reported as standard deviations.

EPR of Mn(II)/RibB. EPR samples (300 μL of the final volume) were prepared by mixing RibB, MnCl₂, and sugar phosphate substrate (D-Ru5P or L-Xy5P) in millimolar ratios (as defined by the experiments, e.g., 3:3:3) in 50 mM Tris-HCl (pH 7.5) and 10% glycerol at 4 °C. Reactions were initiated by the addition of enzyme into the 4 mm quartz EPR tube that contained the metal and sugar phosphate components. The reaction was quenched at the specific times by submerging the EPR tube in liquid nitrogen. X-band EPR data were collected on a 9 GHz Bruker EMXPlus spectrometer. Experiments were run at 10 K with the use of an Oxford ESR900 continuous-flow liquid helium cryostat equipped with an Oxford ITC503 temperature system. Perpendicular-mode data were collected in a dual-mode Bruker ER4116DM cavity. Spectra were recorded using the following non-saturating conditions: 9.64 GHz microwave frequency, 2.0 mW microwave power, 4 G modulation amplitude, 100 kHz modulation frequency, and 40.96 ms time constant.

RibB Crystallization. All crystals were grown at room temperature using the hanging-drop vapor diffusion method. Each drop (3 μL) was prepared by mixing protein and the precipitant solution in equal amounts. Seven crystal structures are described herein [apo-

259 RibB (7UEZ); RibB/D-RuSP (7UF0); RibB/D-RSP/Mn (7UF1);
260 RibB/D-XySP/Mn (7UF2); RibB/L-XySP/2Mn (7UF3); RibB/Int1/
261 Mn (7UF4); and RibB/Int2/Mn (7UF5)]. RibB protein at 40 mg/
262 mL was used to grow cube-shaped apo-RibB crystals using a
263 precipitant solution of 0.1 M $\text{Na}_2\text{HPO}_4/\text{NaH}_2\text{PO}_4$ (pH 9.3), 16%
264 (w/v) PEG 3350, and 0.3 M glycine that reach maximal size in three
265 weeks. These crystals were cryoprotected with 20% PEG (w/v) 3350,
266 5.2 mM D-RuSP, and 0.2 mM MgCl_2 and flash-cooled. The remaining
267 structures were determined from rod-shaped crystals grown using a
268 precipitant solution of 0.1 M lithium acetate and 12–18% (w/v) PEG
269 3350 and reached maximal size in 2 days. The protein concentration
270 for crystal growth was 32.9 mg/mL, and the protein was pre-
271 incubated with the appropriate sugar phosphate prior to drop
272 formation (the sugar phosphate for the intermediate structures was D-
273 RuSP). In all cases, the sugar phosphate was at 15 \times molar excess,
274 except D-RSP. In this case, flakes of D-RSP were added directly to the
275 protein solution. In preparation for data collection, the RibB: D-RSP
276 crystals were transferred to a precipitant solution with 4 mM MnCl_2
277 and 30% (v/v) ethylene glycol. The remaining crystals were soaked in
278 the precipitant solution with 40 mM of a non-substrate sugar
279 phosphate or D-RuSP for the intermediate structures. Just before flash
280 cooling, the crystals were transferred to a cryoprotectant solution
281 which was the precipitant solution with 30% (v/v) ethylene glycol.
282 For the RibB/D-XySP/Mn. RibB/L-XySP/2Mn; RibB/Int1/Mn;
283 RibB/Int2/Mn structures, the cryoprotectant solution also contained
284 4 mM MnCl_2 . For the intermediate 1 structure, the crystal remained
285 in the second soaking solution for 3 min and for the intermediate 2
286 structure for 70 min.

287 **X-ray Crystal Structure Determination.** The X-ray diffraction
288 data for all RibB crystal structures reported were collected at 100 K
289 using the Stanford Synchrotron Radiation Laboratory (SSRL,
290 Stanford, CA) beamlines 12–2 (apo-RibB structure) and 9–2 (all
291 other structures). The software package Blu-Ice^{30,31} was used to
292 collect 1200 oscillation images (0.15 $^\circ$ per image) with an exposure
293 time of 0.2 s. The incident wavelength for the apo-RibB structure was
294 0.8526 Å, and for all remaining structures, it was 0.9795 Å. Data
295 collection and refinement statistics are in Table S1. All phasing
296 solutions were obtained by molecular replacement using PHENIX,
297 Phaser-MR.³² The model for the apo-RibB molecular replacement
298 calculation was PDB:4P8J, whereas all other used 4P8E.²³ The log
299 likelihood gain and TFZ score for each solution are also found in
300 Table S2. Solutions were subjected to alternating cycles of model
301 building and refinement using Coot³³ and Phenix.Refine.^{34,35} Water
302 molecules were added automatically and inspected manually using
303 Coot. All ligands were added manually (sugar phosphates,
304 intermediates, metals, and ethylene glycol) with restraints for the
305 sugar phosphates generated using eLBOW³⁶ and REEL.³⁷ Anisotropic
306 B-factors were only used for the high-resolution apo-RibB structure.
307 The components of the final models (residues, waters, metals, and
308 sugar phosphates) are summarized in Table S2. Structures figures
309 were prepared using Pymol (Schrodinger).

310 **6-Phosphogluconate Dehydrogenase (Ec6PGDH) Prepara-**
311 **tion.** The overexpression construct for the *E. coli* K-12 (ATCC
312 #47076) Ec6PGDH was prepared by GenScript. The gene was
313 synthesized and placed into a pET-28b(+) vector, and the vector was
314 transformed into BL21(DE3) *E. coli*. This overexpression construct
315 yields protein with an N-terminal 6 His tag. The transformed bacteria
316 were grown overnight at 37 $^\circ\text{C}$ in 100 mL of LB broth with 50 $\mu\text{g}/\text{mL}$
317 kanamycin in a shaker incubator (250 rpm). 1L of LB broth with 50
318 $\mu\text{g}/\text{mL}$ kanamycin was inoculated with 35 mL of the overnight culture
319 and grown at 37 $^\circ\text{C}$ in a baffled flask in a shaker incubator (250 rpm).
320 When the culture $\text{OD}_{600\text{nm}}$ reached 0.9, protein expression was
321 induced with a final concentration of 1 mM IPTG and was further
322 incubated at 20 $^\circ\text{C}$ for overnight with shaking. The cells were
323 harvested by centrifugation (6000g, 10 min, 4 $^\circ\text{C}$). The cell pellet was
324 resuspended in 10 mL of 25 mM Tris-HCl (pH 8.0), 50 mM
325 imidazole, and 500 mM NaCl per liter of culture broth. Resuspended
326 cells were lysed by passage through a French Press three times at
327 13,000 psi. The cell lysate was centrifuged at 12,000g for 30 min at 4
328 $^\circ\text{C}$. The supernatant was injected onto a 25 mL Chelating Sepharose

Fast Flow (GE Healthcare) column charged with nickel chloride and
pre-equilibrated with 25 mM Tris-HCl (pH 8.0), 50 mM imidazole,
and 500 mM NaCl. The protein was eluted with a step gradient with
an imidazole concentration of 300 mM imidazole. The fractions
containing the Ec6PGDH were dialyzed into 25 mM Tris-HCl (pH
8.0) and stored for later use at -80 $^\circ\text{C}$. The final yield was 648 mg
per liter of culture, as determined by Bradford analysis.

Preparation of ^{13}C -Labeled Ribulose 5-Phosphate. Singly
and uniformly ^{13}C -labeled D-ribulose 5-phosphate was prepared by
reconstitution of the pentose phosphate pathway following the
published protocol.³⁸ In a final volume of 4 mL, 50 mM Tris-HCl
(pH 7.5), 40 mM MgCl_2 , 40 mM ATP, 37 mM labeled ^{13}C glucose
(Cambridge Isotope Laboratories and Sigma), and 10 mM DTT
(GoldBio) were mixed, and the pH was adjusted to 7.8 using 1 M
NaOH. Hexokinase [60 U, Sigma-Aldrich, *Saccharomyces cerevisiae* (*S.*
cerevisiae)] was added, and the solution was incubated at 37 $^\circ\text{C}$ for 30
min. In a second vial, 4 mL of 75 mM ammonium acetate, 10 mM
NADP $^+$, and 70 mM α -ketoglutarate were mixed, and the pH was
adjusted to 7.8 with 1 M NaOH. The two vials were combined, and
20 μM Ec6PGDH (final concentration), 20 U glutamate dehydrogen-
ase (Sigma-Aldrich, bovine liver), and 12 U glucose 6-phosphate
dehydrogenase (Sigma-Aldrich, *S. cerevisiae*) were added. The
reaction was incubated at 37 $^\circ\text{C}$ for 3 h. Barium chloride, at a final
concentration of 50 mM, was added to the solution. The solution was
mixed and incubated on ice for 5 min. A white precipitate formed and
was pelleted by centrifugation (4300g, 20 min, 4 $^\circ\text{C}$). The
supernatant was incubated in 80% ethanol at -20 $^\circ\text{C}$ for 30 min.
The precipitate was washed in 90% ethanol twice and dried under
nitrogen. The dried white solid was resuspended in 15 mL of water,
and sodium sulfate was added to 100 mM. The white precipitate was
removed by centrifugation (4300g, 20 min, 4 $^\circ\text{C}$). The supernatant
was lyophilized producing a white powder that was resuspended in 50
mM Tris-HCl (pH 8.0). The concentration of D- ^{13}C -RuSP was
determined by colorimetric assay¹⁸ and the standard curve using
unlabeled D-RuSP (Sigma-Aldrich), as previously described. The D-
RuSP was authenticated by ^{13}C NMR using published peak
assignments.¹⁶

Acid-Quenched Single Turnover Monitored by NMR. RibB in
50 mM Tris-HCl (pH 8.0) was concentrated to 120 mg/mL (5.0
mM). The reaction mixture contained 50 mM Tris-HCl (pH 8.0),
20% D_2O , 3 mM MgCl_2 , and 2.8 mM RibB. The reaction was
equilibrated to 4 $^\circ\text{C}$ and initiated by the addition of 2 mM D- ^{13}C -
RuSP. At specific times, 500 μL was withdrawn and quenched by the
addition of 50 μL of 4 M H_2SO_4 . The quenched reaction mixtures
were stored in -20 $^\circ\text{C}$ until NMR data acquisition. All ^{13}C NMR
spectra were recorded on a Bruker Avance III HD (500 MHz)
equipped with a Prodigy CryoProbe at 298 K. ^1H decoupled ^{13}C
spectra (pulse sequence: udef) were recorded with 256 scans, a pre-
acquisition delay of 4 s, and a sweep width of 240 ppm. ^1H coupled
 ^{13}C spectra (pulse sequence: zggd) were recorded with 256 or 4096
scans, a pre-acquisition delay of 3 s, and a sweep width of 250 ppm.
The spectra were referenced based on the published spectra.¹⁶

RESULTS

RibB Production and Activity. *V. cholerae* RibB with an
N-terminal histidine tag was heterologously expressed in *E. coli*
and purified in two chromatographic steps, nickel affinity and
gel filtration. Steady-state kinetic parameters were determined
using colorimetric assay that was originally designed from
high-throughput screening using the *E. coli* isozyme. Assay
measures the production of terminal ketones in the presence of
saturating amounts of creatine and naphthol.^{39,40} However, for
screening, the substrate was developed *in situ* from ribose 5-
phosphate using pentose phosphate isomerase to generate
ribulose 5-phosphate. We have adapted the assay such that we
provide the sugar phosphate of interest directly, using
dihydroxybutanone to generate a standard curve for
quantitation. The assay yielded kinetic parameters when D- 395

396 Ru5P was used as the varied substrate, $k_{\text{cat}} = 2.2 \pm 0.2 \text{ min}^{-1}$;
 397 $K_m = 277 \pm 3 \mu\text{M}$; and $k_{\text{cat}}/K_m = 130 \pm 10 \text{ M}^{-1}\text{s}^{-1}$. When
 398 Mg^{2+} was the varied component, $k_{\text{cat}} = 2.7 \pm 0.4 \text{ min}^{-1}$; $K_m =$
 399 $70 \pm 10 \mu\text{M}$; and $k_{\text{cat}}/K_m = 600 \pm 200 \text{ M}^{-1}\text{s}^{-1}$. When Mn^{2+}
 400 was substituted for Mg^{2+} as the varied component, $k_{\text{cat}} = 0.7 \pm$
 401 0.1 min^{-1} ; $K_m = 11 \pm 1 \mu\text{M}$; and $k_{\text{cat}}/K_m = 1050 \pm 20 \text{ M}^{-1}\text{s}^{-1}$.
 402 This represents an almost two-fold increase in the catalytic
 403 efficiency for Mn^{2+} compared to Mg^{2+} . The Michaelis–Menten
 404 plots are found in Figure S1.

405 **RibB is a Mononuclear Metal Enzyme.** RibB is reported
 406 to be a Mg-dependent enzyme, and crystal structures with a
 407 variety of metals bound (Mg^{2+} , Zn^{2+} , and Ca^{2+}) show two
 408 metal ions in the active site (Figure 2). For this reason,
 409 proposed chemical mechanisms have assumed the involvement
 410 of two Mg^{2+} ions.^{20,21,23,27} To test this assumption, RibB was
 411 titrated with metals (Mg^{2+} , Zn^{2+} , and Mn^{2+}) against a known
 412 concentration of enzyme ($60 \mu\text{M}$), and metal binding was
 413 measured by intrinsic tyrosine fluorescence. Because adventi-
 414 tious metals from protein production and purification were
 415 difficult to remove, the protein was purified in the presence of
 416 $100 \mu\text{M}$ EDTA, and all buffers for these experiments contained
 417 $100 \mu\text{M}$ EDTA. Therefore, assuming EDTA has a higher
 418 affinity for the added metal ions than RibB, a change in
 419 fluorescence is expected once the metal concentration exceeds
 420 $100 \mu\text{M}$, and the change should come to a limit once sufficient
 421 metal is bound that the tyrosine environment is no longer
 422 changing appreciably. The titration experiment shows that
 423 tyrosine fluorescence begins increasing once $100 \mu\text{M}$ metal is
 424 added (the EDTA is saturated) and appears to saturate at
 425 $\sim 160 \mu\text{M}$ (equivalent to the EDTA concentration added to
 426 the protein concentration), keeping in mind the large error of
 427 this low signal assay. In other words, one equivalent of metal
 428 saturates the change in the signal (Figure 3A). A similar
 429 titration was performed measuring activity instead of tyrosine
 430 fluorescence. Activity assay confirms that RibB is inactive in
 431 the presence of Zn^{2+} but active in the presence of Mg^{2+} and
 432 Mn^{2+} and shows that no more than one metal ion is required
 433 for full activity (Figure 3B). One would be tempted to propose
 434 that additional Mn^{2+} ions over 1:1 ratio was inhibitory;
 435 however, after the addition of one equivalent of Mn^{2+} , enzyme
 436 precipitation is observed, which is the likely cause of the
 437 decrease in the activity above $160 \mu\text{M}$ Mn^{2+} . Mn^{2+} has also
 438 been reported to interfere with the color development in
 439 assay.¹⁸

440 Before discussing the EPR spectra for this present system,
 441 we briefly summarize prior relevant EPR studies of Mn-
 442 substituted dinitrogenase reductase. When subjected to EPR,
 443 di-nuclear Mn^{2+} center of dinitrogenase reductase shows
 444 characteristic sets of ^{55}Mn hyperfine lines at 2800G and
 445 3800G with hyperfine splitting of 45G. However, the spectra
 446 also reveal a high intensity six peak pattern at 3400G suggestive
 447 of free Mn^{2+} metal ions in solution (*i.e.*, hexa-aqua Mn^{2+}).⁴¹
 448 Following a similar methodology, we first mixed D-Ru5P with
 449 Mn^{2+} : the spectra showed the high intensity pattern expected
 450 for free Mn^{2+} (black trace, Figure 4). RibB with an equimolar
 451 concentration of Mn^{2+} showed the same six peak pattern but at
 452 significantly lowered intensity, indicating binding of Mn^{2+}
 453 to the protein (blue trace). Equimolar RibB and Mn^{2+} (3 mM)
 454 were mixed with catalytically inactive substrate analogue L-
 455 Xy5P (2 mM) and incubated for 10 min before being freeze-
 456 quenched. This spectrum shows hyperfine splitting of 46G at
 457 2800G and 4000G, characteristic of a di- Mn^{2+} center (dark red
 458 trace). As we will see in the crystal structures described below,

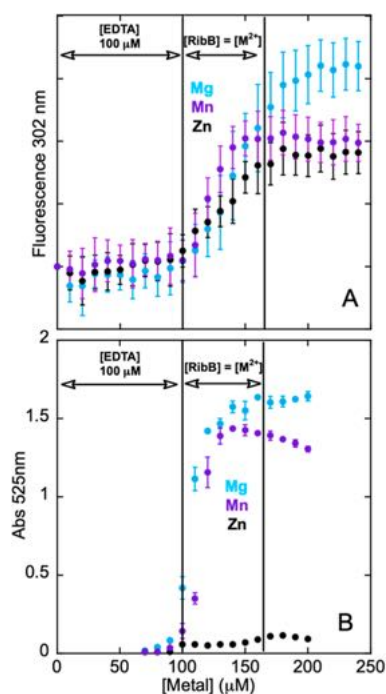


Figure 3. RibB is a mononuclear metal enzyme by binding and activity assays. (A) Intrinsic tyrosine fluorescence shows a 1:1 stoichiometry of metal/RibB for Mg(II), Zn(II), or Mn(II), once the concentration of EDTA is surpassed. (B) Activity assays show one equivalent of Mg(II) or Mn(II) is required for full activity, and that Zn(II) is noncatalytic. [RibB] = $60 \mu\text{M}$, EDTA = $100 \mu\text{M}$.

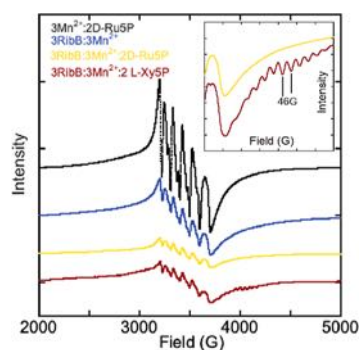


Figure 4. RibB is a mononuclear metal enzyme by EPR. EPR samples were prepared by mixing RibB, MnCl_2 , and sugar phosphate substrate (D-Ru5P or L-Xy5P) in the millimolar ratios shown. The enzyme was added as the final component, and the reaction was quenched by freezing in liquid nitrogen after a 10 min incubation. The non-substrate sugar phosphate L-Xy5P sample shows the characteristic hyperfine splitting for a di-manganese center (inset, brown), whereas the substrate D-Ru5P sample does not exhibit this feature (gold) indicating only one metal in the catalytic site for turnover.

the L-Xy5P structure has a di- Mn^{2+} center. Finally, equimolar
 RibB and Mn^{2+} (3 mM) were mixed with substrate D-Ru5P (2
 mM) and incubated for 10 min (approximately two half-lives
 of the k_{cat} value or 75% complete) before being quenched by
 freezing. Note the characteristic six peak pattern at 3400G
 suggestive of metal binding within the enzyme (gold trace),
 without hyperfine splitting below 3200G, indicating one Mn^{2+}
 in the active complex.

RibB Catalysis is pH Dependent. RibB shows a
 significant decrease in steady-state kinetic parameters at pH

values below pH 7, leading to the initial hypothesis that a catalytic base could be important in the mechanism (Figure 5A). To ensure that the pH dependence of catalytic activity

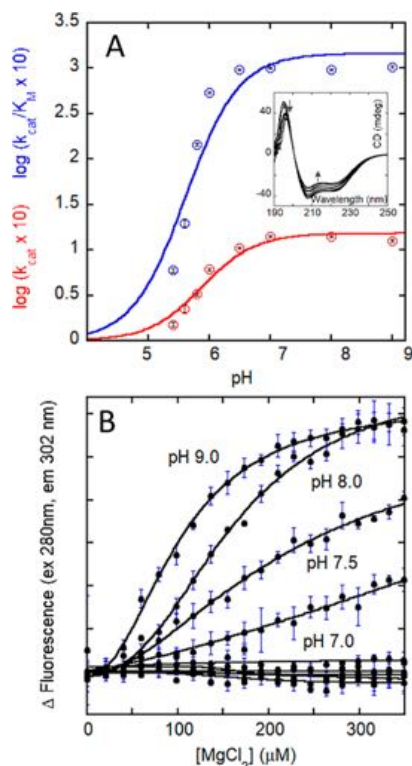


Figure 5. RibB shows a pH dependence for catalytic activity that is associated with the binding of the catalytically required magnesium ion. (A) Steady-state kinetic parameters show a significant decrease in activity at pH values below 7. Inset. RibB maintained a primarily α -helical structure from pH 4 to pH 9, arrows indicate trend with increasing pH. (B) Catalytically required metal only binds to the protein at pH values above pH 6.

was not merely a function of protein folding, circular dichroism spectra were measured from pH 4 to 9, showing that the protein retained a predominantly α -helical fold at all pH values (Figure 5A inset). Magnesium ion-binding isotherms across the same pH range using the tyrosine fluorescence assay showed that the metal ion binds to the enzyme with high affinity at pH values above 7 (Figure 5B). Therefore, the catalytic dependence, as shown in Figure 5A, is associated with the protein's ability to bind the catalytically required magnesium ion. Since the magnesium ion is coordinated by His154, it is tempting to speculate that the pH effect is due to the deprotonation of this residue, providing a lone pair of electrons for metal ion coordination.

Active and Inactive Metal–Substrate Complexes in the RibB Active Site. The enzymatic activity of RibB with different 5-carbon sugar phosphates was compared with their binding modes in the active site. First, the apo-RibB structure was determined to very high resolution (1.08 Å). A representative electron density map is found in Figure S2. The RibB active site is enclosed by two mobile loops. Residues 33–42 comprise Loop 1, which contains Glu39. In the apo-structure, Loop 1 is in an open conformation, with Glu39 pointing away from the active site, unavailable to chelate the metal ion required for catalysis. Residues 83–97 comprise Loop 2, which is disordered in this structure. A second metal

ion chelating residue, His154, is the terminal residue of a helix composed of residues 154–165. This secondary structural element holds the backbone of His154 in place but without sugar phosphate or metal or closed loops 1 and 2, and the side chain has a rotameric conformation that differs from that observed for all other structures solved (Figure 6A).

The structure of RibB was determined with the biological substrate D-ribulose 5-phosphate in the absence of a metal ion (RibB/D-Ru5P; Figure 6B). D-Ru5P binds in an extended conformation similar to that seen in the reported D-Ru5P:2Zn structure, as shown in Figure 2. Both loops 1 and 2 are in their closed conformations in this structure, and Glu39 and His154 are positioned for metal chelation. Crystals of this kind were soaked with Mn²⁺ for the structures of the reaction intermediates, described below. As noted above (and for easy comparison here), when magnesium ions are added, RibB demonstrates a $K_m = 277 \pm 3 \mu\text{M}$ with D-Ru5P. Ribose 5-phosphate (D-R5P) is the aldopentose analogue of the ketopentose biological substrate ribulose 5-phosphate (D-Ru5P). D-R5P is a poor substrate for RibB, with a K_m estimated to be 25–50 mM (Figure S1B, blue). The data do not fit to a Michaelis–Menten model due to significant inhibition at higher concentrations of the substrate. A crystal structure with the sugar phosphate shows a binding mode similar to D-Ru5P and can be trapped in the presence of manganese, chelated as expected in the active site by Glu-39 and His-154 (Figure 6C). The aldopentose D-xylulose 5-phosphate (D-Xy5P) is a better substrate (K_m estimated at 2–3 mM) but with a similar inhibition profile to D-R5P (Figure S1A, dark red). The structure of RibB with Mn²⁺ and D-Xy5P was determined and is shown in Figure 6D. This sugar phosphate binds in a more elongated pose with the hydroxyls of C3 and C4 in an alternate conformation than seen in D-Ru5P and D-R5P, due to the change in chirality at C3. Finally, the structure was determined with the aldopentose L-xylulose 5-phosphate (L-Xy5P), showing two manganese ions and a significantly different, more twisted binding mode (Figure 6E). This sugar phosphate showed no activity at any concentration tested.

Assignment of NMR Spectra of Acid-Quenched RibB D-Ru5P Reactions. The exceptionally slow turnover number of VcRibB at 4 °C provided the opportunity to halt the reaction at specific times and analyze the reaction mixture in a time-dependent manner. The quenched samples were analyzed using ¹³C NMR for both fully labeled D-Ru5P and repeated using substrate singly labeled at each carbon. Figure 7 depicts representative ¹H decoupled ¹³C NMR resonances of the substrate, products, and two distinct reaction states and as such do not represent discrete reaction times.

In this figure, the resonances of individual carbons are color-coded so that the reaction path traversed, and destination of individual carbons is apparent. Overlaid in gray are the ¹H decoupled ¹³C NMR resonances observed for the fully ¹³C-labeled substrate. All NMR spectra including ¹H spectra for singly ¹³C-labeled substrates collected are shown in Figures S3–S12. The assignment based on these spectra are summarized at the right in Figure 7, and the ¹H decoupled-¹³C resonances and multiplicities for the four reaction states observed are listed in Table S3. Definitive assignment of the progression for each carbon was made from the singly ¹³C-labeled substrates (Figures S3–S8); these data show two intermediate states accumulate and decay between 0 and 5 min. Conversion of C1 from an alcohol to a primary alkyl state

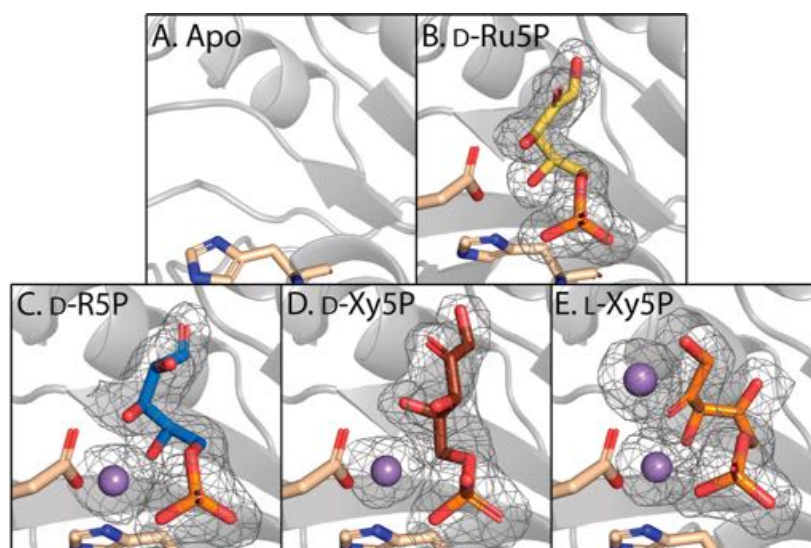


Figure 6. Structures of RibB with sugar phosphates that are substrate analogues show only one metal ion in the active site, and the sugar phosphates bind in an elongated fashion. The RibB structure with a variety of sugar phosphate molecules with metal coordinating residues, Glu39 and His154 shown as wheat colored. (A) RibB was crystallized in the absence of sugar phosphate in an open conformation such that the active site loop containing Glu39 coordinating the metal ion is not visible in this image. (B) Addition of D-Ru5P (yellow sticks) to the crystal orders the active site loop of RibB with an extended conformation of the sugar phosphate, as seen in previous structures. The substrates (C) D-R5P (blue) and (D) D-Xy5P (dark red) have the sugar phosphates in a similar elongated conformation and contain one Mn^{2+} ion in the active site. (E) L-Xy5P (orange) is not a substrate for RibB and binds in the active site in a twisted conformation and coordinates two Mn^{2+} metals. Manganese ions are depicted as purple spheres. The maps are Polder maps contoured at 3σ .⁴²

560 is observed as a 40 ppm upfield shift which is retained as the
 561 molecule is converted to a subsequent intermediate before
 562 resolving to the product. In contrast, C2 retains a resonance
 563 consistent with a ketone throughout the reaction. In the
 564 progression from D-Ru5P to intermediate 1, C3 moves ~ 22
 565 ppm downfield to a chemical shift of 96.2 ppm indicative of a
 566 gem-diol carbon. This is interpreted as a hydration artifact
 567 arising from acid quench and indicates that C3 is likely a
 568 carbonyl in the first transient observed. The resonance for this
 569 carbon moves upfield in the subsequent intermediate state,
 570 revealing its return to an alcohol state, and this state is retained
 571 in the DHBP product. C4 resonates as a hydroxyl bearing
 572 carbon in both the substrate and intermediate 1 states but
 573 moves downfield to resonate as a gem-diol in the second
 574 transient species to then resolves as a formate carboxylate in
 575 the spectrum of the products. For the species observed, the
 576 chemical nature of C5 does not change and thus resonates
 577 within a 2 ppm range throughout the reaction and moreover
 578 exhibits a consistent small 4–5 Hz coupling to the two-bond
 579 distant ^{31}P of the phosphate moiety. The transient species
 580 observed definitively indicate the accumulation and decay of
 581 two intermediate states in single turnover of VcRibB. Neither
 582 of the assigned states definitively identify a single species but
 583 are each consistent with acid quench of two successive states,
 584 shown as boxed in Figure 1.

585 Remarkably, the same two intermediate states are observed
 586 by X-ray crystallography. Crystals grown with the substrate D-
 587 Ru5P were soaked for 3 min in a cryo-protectant solution
 588 containing Mn^{2+} before being plunged in liquid nitrogen to
 589 stop the reaction and prepare the crystal for diffraction. When
 590 this structure was solved, the density of the closed active site is
 591 best modeled to contain 80% substrate (D-Ru5P) and 20% of
 592 intermediate 1, with the 2-keto, 3,3-diol (Figure 7B) produced
 593 by the acid quench NMR experiment, more accurately
 594 depicted as a 2,3-diketone (Figure 8A). Crystals soaked for

70 min in the Mn^{2+} -containing cryo-protectant display density 595
 consistent with 56% Intermediate 2 that was modeled as the 596
 gem-diol. While the acid quench NMR data are consistent with 597
 hydration by the enzyme to make the gem diol, it is also 598
 possible that the acid quench performed the hydration of the 599
 preceding aldehyde intermediate (Figure 1). However, the 600
 crystallographic data shows density consistent with the C4 gem 601
 diol (Figures 1 and 7C). This intermediate is modeled as the 602
 predominant fraction of the density and has the sp^3 C3 603
 somewhat flattened. This geometry is suggestive of strain that 604
 would facilitate formate elimination and formation of the 605
 trigonal planar C3 enol of the DHBP tautomer (Figure 1). The 606
 remaining 44% of the density was fit to the two products, 607
 dihydroxybutanone phosphate and formate (Figure 8B). 608

DISCUSSION

609
 610 The identity of the four-carbon unit required in the 610
 condensation of 5-amino-6-ribitylamino-2,4-pyrimidinedione 611
 to form the xylene moiety of 6,7-dimethyl-8-ribityllumazine in 612
 the biosynthesis of riboflavin was a long-standing matter of 613
 conjecture. In the mid-1950s, Plaut and Broberg demonstrated 614
 that the xylene methyl groups and the carbons to which they 615
 were attached were derived from the C1 and C6 of 616
 glucose.^{43,44} Later intermediates of the butanediol pathway 617
 were implicated,^{45,46} and then, the pentose phosphate pathway 618
 before both were rejected.⁴⁷ Dismutation of the 5-amino-6- 619
 ribitylamino-2,4-pyrimidinedione ring was also proposed, in 620
 which the ribityl was the source of the four carbons.^{48,49} 621
 Eventually, Alworth and co-workers identified the origin of the 622
 methyl groups in the 5,6-dimethylbenzimidazole moiety of 623
 cobalamin as derived from ribose-5-phosphate and given that 624
 the origin of this moiety is from riboflavin, pentose sugar 625
 phosphates were again implicated as the source of the four 626
 carbons.^{50–55} This proposal was later confirmed using ^{13}C 627
 labeling that also revealed that the C6-methyl, C6, and C7 628

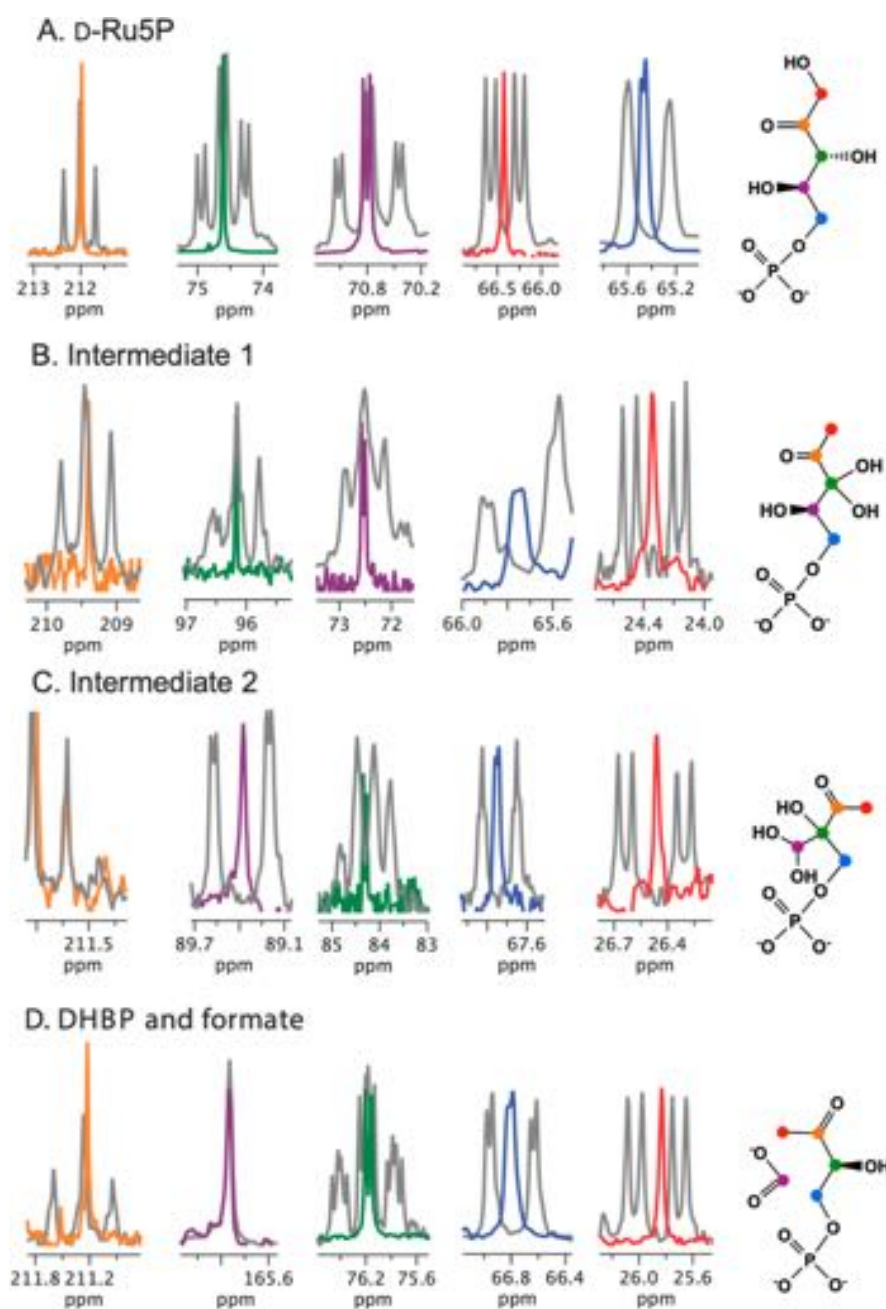


Figure 7. Identification of two reaction intermediates by single turnover NMR. RibB was followed as a single turnover reaction using ^{13}C D-Ru5P and quenched with acid at various time points. The D-Ru5P is converted to DHBP and formate with the transient appearance of two distinct intermediates. Fully labeled ^{13}C (gray) and each singly labeled carbon were followed through the reaction and shown in colors; C1 (red), C2 (orange), C3 (green), C4 (purple), and C5 (blue).

629 came from C1–C3 of pentoses but oddly, the C7-methyl came
 630 from pentose C5.^{12,13,56,57} This was the first evidence that a
 631 rearrangement reaction was required. In 1985, an activity was
 632 identified that formed a 4-carbon product that was a substrate
 633 for lumazine synthase, at last quelling prior notions that a
 634 pentose was the substrate.⁵⁸ Ultimately, D-ribulose 5-phosphate
 635 was recognized as the substrate for this newly identified
 636 enzyme, and the ^{13}C -labeled substrate was used to show that
 637 formate and L-3,4-dihydroxy-2-butanone-4-phosphate were the
 638 products,¹⁵ putting to rest a 35-year biochemical enigma.
 639 Soon after establishment of the reaction, a mechanism was
 640 proposed, in which the skeletal rearrangement of D-ribulose 5-
 641 phosphate was achieved via an anionotropic 1,2-migration such

that the C5 attacks the pentose C3, instigating the elimination
 of C4 as a formate via a gem diol moiety (Figure 1).¹⁶ This
 soundly reasoned mechanism was consistent with labeling and
 incorporation studies that show solvent deuterium incorpo-
 ration at C1 and C3. The canonical mechanism has been
 rewritten in numerous articles since its initial pro-
 posal^{20,21,23,59,60} and once the first structures of RibB were
 published, the mechanistic proposal has been redrawn in the
 context of the active site residues.^{20,28}

These initial X-ray crystal structures were of RibB
 reconstituted with Mg, Mn, or Zn ions and revealed either
 one or two metal ions within the active site.^{19–21,27} Contextual
 chemical mechanisms have generally incorporated two metal

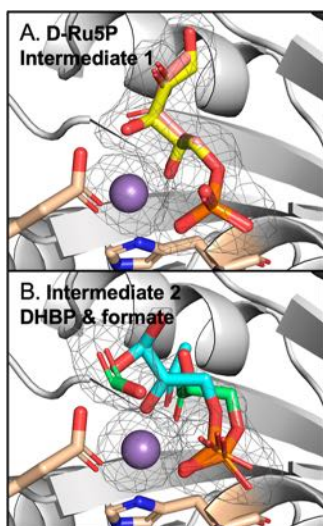


Figure 8. Identification of two reaction intermediates by single turnover X-ray crystallography. (A) RibB crystals were grown with D-ribulose 5-phosphate and soaked with MnCl_2 for 3 min. The map is best modeled with 80% substrate (yellow) and 20% Intermediate 1 as the 2,3-diketone (pink). (B) Crystals soaked for 70 min produced a structure with density that is modeled as 56% intermediate 2 in the gem diol form (cyan) and 44% of the two products, dihydroxybutanone phosphate and formate (green). Both structures show a single manganese ion in the active site (purple). The maps are Polder maps contoured at 3σ .

ions, and this cofactor set has become the accepted native active site configuration. Within RibB, the second metal ion has only two direct coordinating contacts, one with the substrate C2 carbonyl and one with Glu39. In contrast, the metal ion liganded to the substrate C3 and C4 hydroxyl groups, and the terminal phosphate of D-Ru5P is also coordinated to His154 and Glu39 (VcRibB residue numbers).²¹ In each case, the structures solved with two metal ions were either of a vestigial, non-active form of RibB or were

solved when liganded to substrate analogue sugar phosphates and so do not depict a native state of the enzyme. Moreover, in each case, when the chemical mechanism of RibB has been presented, it has rightly been described as hypothetical as little direct evidence for the chemical species involved in the reaction was available. We present the first direct evidence for the mechanism of RibB. These data show that the general reasoning of the canonical mechanism by Bacher *et al.* holds, but that it is achieved with the involvement of a single active site metal ion.

The slow turnover rate of VcRibB facilitated acid quench of the reaction, and selective ^{13}C -labeling of D-Ru5P via reconstitution of the pentose phosphate pathway gave the means for unambiguous assignment of the origin and destination of all carbons that constitute two transient species observed to accumulate under single turnover conditions (Figure 7). These data indicate elimination of the C1-hydroxyl from an ene-diol species to form a 2,3-diketone that is observed to accumulate with acid quench in the hydrated 2-keto, 3,3-diol state (Figure 9). With regard to the chemical mechanism, this localizes the quenched intermediate to either the 1-ene-2-ol-3-one species or the ensuing 2,3-diketone. The subsequent transient liberated in acid quench is the result of rearrangement and has the C5 bonded to C3 with C4 as a gem diol that is poised for elimination as formate. This is the first observation of this fundamental RibB transient, and confirmation of its existence arguably dictates much of the preceding and subsequent chemistry in the RibB catalytic cycle.

One primary role of the magnesium (or manganese) ion in RibB is Lewis acidity, stabilizing hydroxide states of coordinated hydroxyls and waters, thereby inducing tautomerizations, hydration, and two elimination reactions. It is not immediately apparent that a second metal ion is required to accomplish this chemistry, and each structure of VcRibB solved with a substrate or intermediate state bound that we present here has only one metal ion, and full activity is achieved with equimolar Mg or Mn (Figure 5). While this

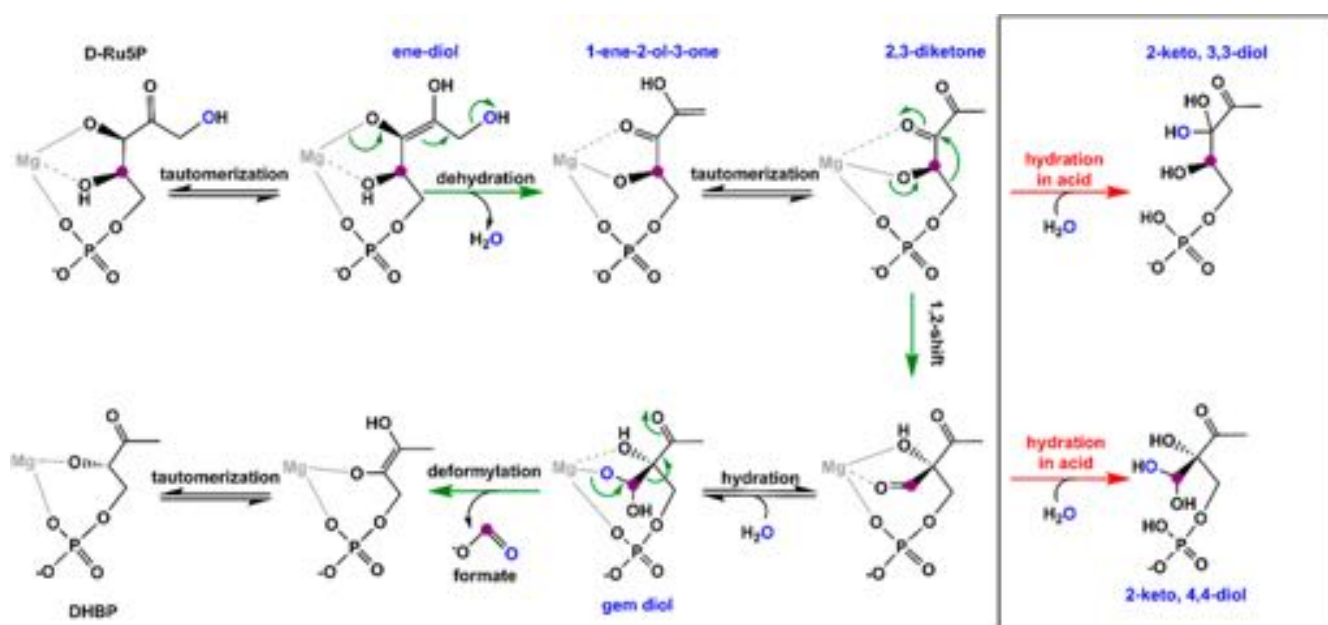


Figure 9. Evidence-based mechanism. Boxed reactions indicate hydrated acid-quenched products identified in the NMR data.

702 observation does not rule out transient involvement of a
703 rapidly exchanging second metal ion amid relative slow
704 chemistry, it does indicate that one metal ion has a dominant
705 role and anchors substrate binding and much of the catalytic
706 cycle. In Figure 8, we show density for a single metal ion in two
707 states of catalysis representative of four distinct species,
708 modeled as a 4:1 ratio of the ES complex and the 2,3-diketone
709 intermediate (intermediate 1), and the rearranged and
710 hydrated intermediate (intermediate 2) added to a roughly
711 equal fraction of the product complex.

712 Structures of VcRibB with the native substrate, D-Ru5P, were
713 solved in the presence of Mn ions that induce even slower rates
714 of turnover (Figure 8). The structure of the VcRibB-Mn-D-
715 Ru5P complex has the metal ion coordinated to the C3 and C4
716 hydroxyl substituents and the phosphate of the substrate.
717 Within a 3 min incubation period, the reaction advances in
718 crystallo to partial elimination of the C2-hydroxyl retaining
719 coordination to the same oxygen atoms presumably with the
720 C3 now in the keto state and the tautomeric state of the C1-
721 C2 enol/keto group unknown. The observed conformation of
722 intermediate 1 when best fit to the available density at 2.2 Å
723 resolution indicates a Bürgi-Dunitz angle within 10° of
724 optimal for the nucleophilic attack of C5 on C3. This
725 conformation has an altitude 117° and an azimuth 145° across
726 a gap of 2.4 Å,⁶¹ a geometry that promotes the migration
727 reaction that forms intermediate 2 (Figure 8A). The exact
728 mechanism of migration is not apparent from these data. Shifts
729 of this type are analogous to Pinacol rearrangements where
730 migration is induced by an adjacent carbonium ion.⁶² At this
731 stage of catalysis, the Lewis acidity of the metal ion of RibB
732 presumably works to denude the C3 carbonyl carbon of
733 electrons increasing its electrophilicity. Whether the migration
734 is concerted and involves a single transition state with partial
735 bonding of C5 to both C4 and C3 or stepwise with the
736 formation of a C5 carbanion is a nuanced chemical argument
737 that is beyond the reach of the data presented. However, the
738 first definitive observation of the predicted migration product
739 (intermediate 2) confines the mechanistic possibilities
740 considerably and confirms an otherwise unsubstantiated
741 mechanism first proposed in 1991.¹⁶

742 The crystallographic intermediate 2 state, as shown in Figure
743 8B, has density for the C4 gem diol. This is therefore the same
744 as the species observed as the second transient in acid quench
745 NMR data (Figure 7), indicating that the decay of the gem diol
746 to form formate and the enol form of the DHBP product is the
747 rate-limiting chemical step. The product complex includes
748 density for formate and DHBP and is the first experimental
749 observation of these products formed *in situ*.

750 ■ CONCLUSIONS

751 31 years after the initial hypothetical chemical mechanism for
752 RibB was offered, definitive evidence for the accumulation,
753 decay, and chemical identity of two sequential transients is
754 presented. These data indicate that the fundamental steps of
755 1,2-shift of carbon-five and formate elimination from a gem
756 diol bonded to a quaternary carbon-three define the salient and
757 unique catalytic steps of the enzyme's catalytic cycle.

758 ■ ASSOCIATED CONTENT

759 SI Supporting Information

760 The Supporting Information is available free of charge at
761 <https://pubs.acs.org/doi/10.1021/jacs.2c03376>.

Additional crystallographic details; steady-state kinetics; 762
NMR time-course data; proton-coupled NMR data; 763
chemical shifts; and coupling constants for intermediate 764
states (PDF) 765

766 ■ AUTHOR INFORMATION

767 Corresponding Author

Audrey L. Lamb – Department of Molecular Biosciences, 768
University of Kansas, Lawrence, Kansas 66045, United 769
States; Department of Chemistry, University of Texas at San 770
Antonio, San Antonio, Texas 78249, United States; 771
orcid.org/0000-0002-2352-2130; Email: [audrey.lamb@](mailto:audrey.lamb@utsa.edu) 772
utsa.edu 773

774 Authors

Nikola Kenjic – Department of Molecular Biosciences, 775
University of Kansas, Lawrence, Kansas 66045, United 776
States; orcid.org/0000-0002-2871-7674 777

Kathleen M. Meneely – Department of Molecular Biosciences, 778
University of Kansas, Lawrence, Kansas 66045, United 779
States; Department of Chemistry, University of Texas at San 780
Antonio, San Antonio, Texas 78249, United States; 781
orcid.org/0000-0002-0372-9695 782

Daniel J. Wherritt – Department of Chemistry, University of 783
Texas at San Antonio, San Antonio, Texas 78249, United 784
States; orcid.org/0000-0002-8616-9864 785

Melissa C. Denler – Department of Chemistry, University of 786
Kansas, Lawrence, Kansas 66045, United States; 787
orcid.org/0000-0003-2443-6178 788

Timothy A. Jackson – Department of Chemistry, University of 789
Kansas, Lawrence, Kansas 66045, United States; 790
orcid.org/0000-0002-3529-2715 791

Graham R. Moran – Department of Chemistry and 792
Biochemistry, University of Loyola, Chicago, Illinois 60660, 793
United States; orcid.org/0000-0002-6807-1302 794

Complete contact information is available at: 795
<https://pubs.acs.org/doi/10.1021/jacs.2c03376> 796

797 Funding

This publication was made possible by funds from NIH Grants 798
R01 GM127655 and NSF grant 1904494/2041047 to A.L.L. 799
and the University of Kansas General Research Fund. G.R.M. 800
was supported by NSF Grant 1904480 and the Loyola 801
University College of Arts and Sciences. N.K. was supported 802
by the Weaver International Fellowship. M.C.D. was supported 803
by the National Institutes of Health Graduate Training 804
Program in the Dynamic Aspects of Chemical Biology (T32 805
GM008545). The content is solely the responsibility of the 806
authors and does not necessarily represent the official views of 807
the National Institute of General Medical Sciences or the 808
National Institutes of Health. 809

810 Notes

The authors declare no competing financial interest. 811

812 ■ ACKNOWLEDGMENTS

Use of the Stanford Synchrotron Radiation Lightsource, SLAC 813
National Accelerator Laboratory, is supported by the U.S. 814
Department of Energy, Office of Science, Office of Basic 815
Energy Sciences under Contract DE-AC02-76SF00515. The 816
Stanford Synchrotron Radiation Lightsource Structural Mo- 817
lecular Biology Program is supported by the U.S. Department 818
of Energy Office of Biological and Environmental Research and 819

820 by NIGMS, the National Institutes of Health Grant
821 P41GM103393. We thank the staff at the Stanford
822 Synchrotron Radiation Laboratory for their support and
823 assistance. We are grateful to Justin T. Douglas and Sarah A.
824 Neuenswander of the University of Kansas NMR facility for
825 support and assistance. The authors would also like to express
826 thanks to James Devery of the Loyola University Chicago for
827 helpful discussions regarding rearrangement mechanisms.

828 ■ REFERENCES

- 829 (1) Thakur, K.; Tomar, S. K.; Singh, A. K.; Mandal, S.; Arora, S.
830 Riboflavin and health: A review of recent human research. *Crit. Rev.*
831 *Food Sci. Nutr.* **2017**, *57*, 3650–3660.
- 832 (2) Bacher, A.; Eberhardt, S.; Fischer, M.; Kis, K.; Richter, G.
833 Biosynthesis of vitamin B2 (riboflavin). *Annu. Rev. Nutr.* **2000**, *20*,
834 153–167.
- 835 (3) Powers, H. J.; Weaver, L. T.; Austin, S.; Beresford, J. K. A
836 proposed intestinal mechanism for the effect of riboflavin deficiency
837 on iron loss in the rat. *Br. J. Nutr.* **1993**, *69*, 553–561.
- 838 (4) Thiagarajan, V.; Byrdin, M.; Eker, A. P. M.; Müller, P.; Brettel,
839 K. Kinetics of cyclobutane thymine dimer splitting by DNA
840 photolyase directly monitored in the UV. *Proc. Natl. Acad. Sci.*
841 *U.S.A.* **2011**, *108*, 9402–9407.
- 842 (5) Lakshmi, R.; Lakshmi, A. V.; Divan, P. V.; Bamji, M. S. Effect of
843 riboflavin or pyridoxine deficiency on inflammatory response. *Indian J.*
844 *Biochem. Biophys.* **1991**, *28*, 481–484.
- 845 (6) Schramm, M.; Wiegmann, K.; Schramm, S.; Gluschko, A.; Herb,
846 M.; Utermöhlen, O.; Krönke, M. Riboflavin (vitamin B2) deficiency
847 impairs NADPH oxidase 2 (Nox2) priming and defense against
848 *Listeria monocytogenes*. *Eur. J. Immunol.* **2014**, *44*, 728–741.
- 849 (7) Long, Q.; Ji, L.; Wang, H.; Xie, J. Riboflavin biosynthetic and
850 regulatory factors as potential novel anti-infective drug targets. *Chem.*
851 *Biol. Drug Des.* **2010**, *75*, 339–347.
- 852 (8) Sassetti, C. M.; Boyd, D. H.; Rubin, E. J. Genes required for
853 mycobacterial growth defined by high density mutagenesis. *Mol.*
854 *Microbiol.* **2003**, *48*, 77–84.
- 855 (9) Mack, M.; Grill, S. Riboflavin analogs and inhibitors of riboflavin
856 biosynthesis. *Appl. Microbiol. Biotechnol.* **2006**, *71*, 265–275.
- 857 (10) Bacher, A.; Le Van, Q.; Buhler, M.; Keller, P.J.; Eimicke, V.;
858 Floss, H. G. Biosynthesis of riboflavin. Incorporation of D-
859 [1-¹³C]Ribose. *J. Am. Chem. Soc.* **1982**, *104*, 3753–3755.
- 860 (11) Bacher, A.; Le Van, Q.; Keller, P. J.; Floss, H. G. Biosynthesis of
861 riboflavin. Incorporation of ¹³C-labeled precursors into the xylene
862 ring. *J. Biol. Chem.* **1983**, *258*, 13431–13437.
- 863 (12) Bacher, A.; Le Van, Q. L.; Keller, P. J.; Floss, H. G. Biosynthesis
864 of riboflavin. Incorporation of multiply ¹³C-labeled precursors into the
865 xylene ring. *J. Am. Chem. Soc.* **1985**, *107*, 6380–6385.
- 866 (13) Le Van, Q.; Keller, P. J.; Bown, D. H.; Floss, H. G.; Bacher, A.
867 Biosynthesis of riboflavin in *Bacillus subtilis*: origin of the four-carbon
868 moiety. *J. Bacteriol.* **1985**, *162*, 1280–1284.
- 869 (14) Volk, R.; Bacher, A. Biosynthesis of riboflavin. The structure of
870 the four-carbon precursor. *J. Am. Chem. Soc.* **1988**, *110*, 3651–3653.
- 871 (15) Volk, R.; Bacher, A. Studies on the 4-carbon precursor in the
872 biosynthesis of riboflavin. Purification and properties of L-3,4-
873 dihydroxy-2-butanone-4-phosphate synthase. *J. Biol. Chem.* **1990**,
874 *265*, 19479–19485.
- 875 (16) Volk, R.; Bacher, A. Biosynthesis of riboflavin. Studies on the
876 mechanism of L-3,4-dihydroxy-2-butanone 4-phosphate synthase. *J.*
877 *Biol. Chem.* **1991**, *266*, 20610–20618.
- 878 (17) Kelly, M. J. S.; Ball, L. J.; Krieger, C.; Yu, Y.; Fischer, M.;
879 Schiffmann, S.; Schmieder, P.; Kühne, R.; Bermel, W.; Bacher, A.;
880 Richter, G.; Oschkinat, H. The NMR structure of the 47-kDa dimeric
881 enzyme 3,4-dihydroxy-2-butanone-4-phosphate synthase and ligand
882 binding studies reveal the location of the active site. *Proc. Natl. Acad.*
883 *Sci. U.S.A.* **2001**, *98*, 13025–13030.
- 884 (18) Piccollelli, M. A.; Viitanen, P. V.; Jordan, D. B. Spectropho-
885 tometric determination of 3, 4-dihydroxy-2-butanone-4-phosphate
886 synthase activity. *Biochem.* **2000**, *287*, 347–349.
- (19) Liao, D.-I.; Calabrese, J. C.; Wawrzak, Z.; Viitanen, P. V.; 887
Jordan, D. B. Crystal structure of 3,4-dihydroxy-2-butanone 4- 888
phosphate synthase of riboflavin biosynthesis. *Structure* **2001**, *9*, 889
11–18. 890
- (20) Liao, D.-I.; Zheng, Y.-J.; Viitanen, P. V.; Jordan, D. B. Structural 891
definition of the active site and catalytic mechanism of 3,4-dihydroxy- 892
2-butanone-4-phosphate synthase. *Biochemistry* **2002**, *41*, 1795–1806. 893
- (21) Steinbacher, S.; Schiffmann, S.; Richter, G.; Huber, R.; Bacher, 894
A.; Fischer, M. Structure of 3,4-dihydroxy-2-butanone 4-phosphate 895
synthase from *Methanococcus jannaschii* in complex with divalent 896
metal ions and the substrate ribulose 5-phosphate: implications for 897
the catalytic mechanism. *J. Biol. Chem.* **2003**, *278*, 42256–42265. 898
- (22) consortium, P. D.-K. PDBe-, KB a community-driven resource 899
for structural and functional annotations. *Nucleic Acids Res.* **2020**, *48*, 900
D344–D353. 901
- (23) Islam, Z.; Kumar, A.; Singh, S.; Salmon, L.; Karthikeyan, S. 902
Structural basis for competitive inhibition of 3,4-dihydroxy-2- 903
butanone-4-phosphate synthase from *Vibrio cholerae*. *J. Biol. Chem.* 904
2015, *290*, 11293–11308. 905
- (24) Singh, M.; Kumar, P.; Yadav, S.; Gautam, R.; Sharma, N.; 906
Karthikeyan, S. The crystal structure reveals the molecular mechanism 907
of bifunctional 3,4-dihydroxy-2-butanone 4-phosphate synthase/GTP 908
cyclohydrolase II (Rv1415) from *Mycobacterium tuberculosis*. *Acta* 909
Crystallogr., Sect. D: Biol. Crystallogr. **2013**, *69*, 1633–1644. 910
- (25) Liao, D. I.; Viitanen, P. V.; Jordan, D. B. Cloning, expression, 911
purification and crystallization of dihydroxybutanone phosphate 912
synthase from *Magnaporthe grisea*. *Acta Crystallogr., Sect. D: Biol.* 913
Crystallogr. **2000**, *56*, 1495–1497. 914
- (26) Steinbacher, S.; Schiffmann, S.; Bacher, A.; Fischer, M. Metal 915
sites in 3,4-dihydroxy-2-butanone 4-phosphate synthase from 916
Methanococcus jannaschii in complex with the substrate ribulose 5- 917
phosphate. *Acta Crystallogr., Sect. D: Biol. Crystallogr.* **2004**, *60*, 1338– 918
1340. 919
- (27) Kumar, P.; Singh, M.; Gautam, R.; Karthikeyan, S. Potential 920
anti-bacterial drug target: structural characterization of 3,4-dihydroxy- 921
2-butanone-4-phosphate synthase from *Salmonella typhimurium* LT2. 922
Proteins **2010**, *78*, 3292–3303. 923
- (28) Echt, S.; Bauer, S.; Steinbacher, S.; Huber, R.; Bacher, A.; 924
Fischer, M. Potential anti-infective targets in pathogenic yeasts: 925
structure and properties of 3,4-dihydroxy-2-butanone 4-phosphate 926
synthase of *Candida albicans*. *J. Mol. Biol.* **2004**, *341*, 1085–1096. 927
- (29) Newman, J. Novel buffer systems for macromolecular 928
crystallization. *Acta Crystallogr., Sect. D: Biol. Crystallogr.* **2004**, *60*, 929
610–612. 930
- (30) McPhillips, T. M.; McPhillips, S. E.; Chiu, H.-J.; Cohen, A. E.; 931
Deacon, A. M.; Ellis, P. J.; Garman, E.; Gonzalez, A.; Sauter, N. K.; 932
Phizackerley, R. P.; Soltis, S. M.; Kuhn, P. Blu-Ice and the Distributed 933
Control System: software for data acquisition and instrument control 934
at macromolecular crystallography beamlines. *J. Synchrotron Radiat.* 935
2002, *9*, 401–406. 936
- (31) Soltis, S. M.; Cohen, A. E.; Deacon, A.; Eriksson, T.; González, 937
A.; McPhillips, S.; Chui, H.; Dunten, P.; Hollenbeck, M.; Mathews, I.; 938
Miller, M.; Moorhead, P.; Phizackerley, R. P.; Smith, C.; Song, J.; van 939
dem Bedem, H.; Ellis, P.; Kuhn, P.; McPhillips, T.; Sauter, N.; Sharp, 940
K.; Tsyba, I.; Wolf, G. New paradigm for macromolecular 941
crystallography experiments at SSRL: automated crystal screening 942
and remote data collection. *Acta Crystallogr., Sect. D* **2008**, *64*, 1210– 943
1221. 944
- (32) McCoy, A. J.; Grosse-Kunstleve, R. W.; Adams, P. D.; Winn, M. 945
D.; Storoni, L. C.; Read, R. J. Phaser crystallographic software. *J. Appl.* 946
Crystallogr. **2007**, *40*, 658–674. 947
- (33) Emsley, P.; Lohkamp, B.; Scott, W. G.; Cowtan, K. Features 948
and development of Coot. *Acta Crystallogr., Sect. D: Biol. Crystallogr.* 949
2010, *66*, 486–501. 950
- (34) Adams, P. D.; Afonine, P. V.; Bunkoczi, G.; Chen, V. B.; Davis, 951
I. W.; Echols, N.; Headd, J. J.; Hung, L. W.; Kapral, G. J.; Grosse- 952
Kunstleve, R. W.; McCoy, A. J.; Moriarty, N. W.; Oeffner, R.; Read, R. 953
J.; Richardson, D. C.; Richardson, J. S.; Terwilliger, T. C.; Zwart, P. 954
H. PHENIX: a comprehensive Python-based system for macro- 955

- 956 molecular structure solution. *Acta Crystallogr., Sect. D: Biol. Crystallogr.*
957 **2010**, *66*, 213–221.
- 958 (35) Afonine, P. V.; Grosse-Kunstleve, R. W.; Echols, N.; Headd, J.
959 J.; Moriarty, N. W.; Mustyakimov, M.; Terwilliger, T. C.; Urzhumtsev,
960 A.; Zwart, P. H.; Adams, P. D. Towards automated crystallographic
961 structure refinement with phenix.refine. *Acta Crystallogr., Sect. D: Biol.*
962 *Crystallogr.* **2012**, *68*, 352–367.
- 963 (36) Moriarty, N. W.; Grosse-Kunstleve, R. W.; Adams, P. D.
964 electronic Ligand Builder and Optimization Workbench (eLBOW): a
965 tool for ligand coordinate and restraint generation. *Acta Crystallogr.,*
966 *Sect. D: Biol. Crystallogr.* **2009**, *65*, 1074–1080.
- 967 (37) Moriarty, N. W.; Draizen, E. J.; Adams, P. D. An editor for the
968 generation and customization of geometry restraints. *Acta Crystallogr.,*
969 *Sect. D: Struct. Biol.* **2017**, *73*, 123–130.
- 970 (38) Richter, G.; Krieger, C.; Volk, R.; Kis, K.; Ritz, H.; Götze, E.;
971 Bacher, A. Biosynthesis of riboflavin: 3,4-dihydroxy-2-butanone-4-
972 phosphate synthase[34] Biosynthesis of riboflavin: 3,4-dihydroxy-2-
973 butanone-4-phosphate synthase. *Methods Enzymol.* **1997**, *280*, 374–
974 382.
- 975 (39) Westerfeld, W. W. A Colorimetric Determination of Blood
976 Acetion. *J. Biol. Chem.* **1945**, *161*, 495–502.
- 977 (40) Speckman, R. A.; Collins, E. B. Specificity of the Westfield
978 adaptation of the Voges - Proskauer test. *Appl. Environ. Microbiol.*
979 **1982**, *44*, 40–43.
- 980 (41) Antharavally, B. S.; Poyner, R. R.; Ludden, P. W. EPR Spectral
981 Evidence for Binuclear Mn(II) Center in Dintorgenase Reductase-
982 Activating Glycohydrolase from *Rhodospirillum rubrum*. *J. Am. Chem.*
983 *Soc.* **1998**, *120*, 8897–8898.
- 984 (42) Liebschner, D.; Afonine, P. V.; Moriarty, N. W.; Poon, B. K.;
985 Sobolev, O. V.; Terwilliger, T. C.; Adams, P. D. Polder maps:
986 improving OMIT maps by excluding bulk solvent. *Acta Crystallogr.,*
987 *Sect. D: Struct. Biol.* **2017**, *73*, 148–157.
- 988 (43) Plaut, G. W. E. Biosynthesis of riboflavin. II. Incorporation of
989 C14-labeled compounds into ring A. *J. Biol. Chem.* **1954**, *211*, 111–
990 116.
- 991 (44) Plaut, G. W. E.; Broberg, P. L. Biosynthesis of riboflavin. III.
992 Incorporation of C14-labeled compounds into the ribityl side chain. *J.*
993 *Biol. Chem.* **1956**, *219*, 131–138.
- 994 (45) Bryn, K.; Stormer, F. Decreased riboflavin formation in mutants
995 of *Aerobacter* (*Enterobacter*) *aerogenes* deficient in the butanediol
996 pathway. *Biochim. Biophys. Acta* **1976**, *428*, 257–259.
- 997 (46) Nakajima, K.; Mitsuda, H. Possibility of diacetyl and related
998 compounds as the 4-carbon compound necessary for the formation of
999 riboflavin in *Ashbya gossypii*. *Acta Vitaminol. Enzymol.* **1984**, *6*, 271–
1000 282.
- 1001 (47) Jabasini, M. T.; Al-Khalidi, U. A. S. Asymmetric labelling of the
1002 xylene ring in riboflavin. *Int. J. Biochem.* **1975**, *6*, 735–739.
- 1003 (48) Bresler, S. E.; Perumov, D. A.; Chernik, T. P.; Skvortsova, A. P.
1004 [Operon for riboflavin synthesis in *Bacillus subtilis*. XI. Determination
1005 of the type of regulation using a test for dominance of operator-
1006 constitutive and regulator-constitutive mutations]. *Genetika* **1976**, *12*,
1007 124–130.
- 1008 (49) Hollander, I. J.; Braman, J. C.; Brown, G. M. Biosynthesis of
1009 riboflavin: enzymatic conversion of 5-amino-2,4-dioxy-6-ribitylamino-
1010 pyrimidine to 6,7-dimethyl-8-ribityllumazine. *Biochem. Biophys. Res.*
1011 *Commun.* **1980**, *94*, 515–521.
- 1012 (50) Alworth, W. L.; Dove, M. F.; Baker, H. N. Biosynthesis of the
1013 dimethylbenzene moiety of riboflavin and dimethylbenzimidazole:
1014 evidence for the involvement of C-1 of a pentose as a precursor.
1015 *Biochemistry* **1977**, *16*, 526–531.
- 1016 (51) Horig, J.; Renz, P. Biosynthesis of vitamin B12. Formation of
1017 free 5,6-dimethylbenzimidazole and alpha-ribazole from riboflavin by
1018 *Propionibacterium freudenreichii*. *FEBS Lett.* **1977**, *80*, 337–339.
- 1019 (52) Horig, J. A.; Renz, P.; Heckmann, G. [5-15N]Riboflavin as
1020 precursor in the biosynthesis of the 5,6-dimethylbenzimidazole
1021 moiety of vitamin B12. A study by 1H and 15N magnetic resonance
1022 spectroscopy. *J. Biol. Chem.* **1978**, *253*, 7410–7414.
- (53) Kühnle, H. F.; Renz, P. Biosynthesis of 5,6-dimethylbenzimi- 1023
dazole. Precursor-function of 6,7-dimethyl-8-ribityllumazine. *Z.* 1024
Naturforsch., B **1971**, *26*, 1017–1020.
- (54) Renz, P. Riboflavin as precursor in the biosynthesis of the 5,6- 1025
Dimethylbenzimidazole-moiety of vitamin B(12). *FEBS Lett.* **1970**, *6*, 1027
187–189. 1028
- (55) Renz, P.; Weyhenmeyer, R. Biosynthesis of 5, 6-dimethylbenzi- 1029
midazole from riboflavin Transformation of C-1' of riboflavin into C- 1030
2 of 5, 6-dimethylbenzimidazole. *FEBS Lett.* **1972**, *22*, 124–126. 1031
- (56) Bacher, A.; Levan, Q.; Buehler, M.; Keller, P. J.; Eimicke, V.; 1032
Floss, H. G. Biosynthesis of Riboflavin—Incorporation of D-[1-C- 1033
13]-Labeled Ribose. *J. Am. Chem. Soc.* **1982**, *104*, 3754–3755. 1034
- (57) Floss, H. G.; Quang Le Van, Q.; Keller, P. J.; Bacher, A. 1035
Biosynthesis of Riboflavin - an Unusual Rearrangement in the 1036
Formation of 6,7-Dimethyl-8-Ribityllumazine. *J. Am. Chem. Soc.* **1983**, 1037
105, 2493–2494. 1038
- (58) Neuberger, G.; Bacher, A. Biosynthesis of riboflavin. An 1039
aliphatic intermediate in the formation of 6,7-dimethyl-8-ribitylluma- 1040
zine from pentose phosphate. *Biochem. Biophys. Res. Commun.* **1985**, 1041
127, 175–181. 1042
- (59) Fischer, M.; Römisch, W.; Schiffmann, S.; Kelly, M.; Oschkinat, 1043
H.; Steinbacher, S.; Huber, R.; Eisenreich, W.; Richter, G.; Bacher, A. 1044
Biosynthesis of riboflavin in archaea studies on the mechanism of 3,4- 1045
dihydroxy-2-butanone-4-phosphate synthase of *Methanococcus jan-* 1046
naschii. *J. Biol. Chem.* **2002**, *277*, 41410–41416. 1047
- (60) Richter, G.; Kelly, M.; Krieger, C.; Yu, Y.; Bermel, W.; Karlsson, 1048
G.; Bacher, A.; Oschkinat, H. NMR studies on the 46-kDa dimeric 1049
protein, 3,4-dihydroxy-2-butanone 4-phosphate synthase, using 2H, 1050
13C, and 15N-labelling. *Eur. J. Biochem.* **1999**, *261*, 57–65. 1051
- (61) Bürgi, H. B.; Dunitz, J. D.; Lehn, J. M.; Wipff, G. 1052
Stereochemistry of reaction paths at carbonyl centres. *Tetrahedron* 1053
1974, *30*, 1563–1572. 1054
- (62) Nakamura, K.; Osamura, Y. Theoretical-Study of the Reaction- 1055
Mechanism and Migratory Aptitude of the Pinacol Rearrangement. *J.* 1056
Am. Chem. Soc. **1993**, *115*, 9112–9120. 1057